INTERNATIONAL SOCIETY FOR SOIL MECHANICS AND GEOTECHNICAL ENGINEERING

SIMSG   ISSMGE

2T3C apparatus and DIC technology to investigate the thermomechanical behaviour of the interface between bituminous layers

Thien Nhan Tran[1#], *Salvatore* Mangiafico[1], *Cédric* Sauzéat[1], and *Hervé* Di Benedetto[1]

[1] *Univ Lyon, ENTPE, Ecole Centrale de Lyon, CNRS, LTDS, UMR5513, 69518 Vaulx en Velin, France*
[#]*Corresponding author: thiennhan.tran@entpe.fr*

ABSTRACT

The bonding at the interface is seen in most road structure design methods as perfectly bonded and this ideal condition is supposed to last during the whole service life. However, the real working capacity at the interface is complex and gradually degrades because of repeated traffic load and weather conditions. A new apparatus called 2T3C ("Torsion, Traction, Compression sur Cylindre Creux" in French, or "Torsion, Tension, Compression on Hollow Cylinder" in English) was developed at the ENTPE/University of Lyon to investigate the thermomechanical behaviour of the interface between bituminous layers. The sample has two layers of similar or different materials. It has a total height of 125 mm and a wall thickness of the 25mm. The thickness was chosen small enough in order to validate the assumption of quasi-homogenous stress and strain fields between inner and outer surface. The DIC technology is performed considering the three listed elements: (1) two couple of cameras are situated on two opposite sides of the sample (4 cameras in total) to take 3D images; (2) a software is employed to calculate the displacements in 3 dimensions of all points in the area of interest; and (3) the strain fields in the 2 layers and the displacement gap at the interface are computed using a method developed at the University of Lyon/ENTPE. In this paper, a focus is proposed on the viscoelastic and fatigue behaviours of the two bituminous layers and of the interface. Small and large numbers of loading cycles are successively considered in the small strain domain.

Keywords: bituminous interlayer, DIC technology, viscoelastic, fatigue

1. Introduction

In a flexible pavement structure, emulsified bitumen is used to bind adjacent asphalt layers together. The layers are designed to be perfectly bonded. Therefore, a solid bonding capacity of the tack coat at the interface plays a key role in ensuring the lifespan of a pavement structure. Due to the traffic loading and weather effects, the quality of the tack coat reduces gradually, which can lead to premature failures or degradation of the whole structure. The perfect bonding at the interface is probably not maintained during the service life, as considered in most of the design methods.

The need to better understand the actual behaviour at the interface has been studied with different apparatuses. These devices are able to apply monotonic or cyclic shear loading combined with different temperatures and loading rates on samples. It is worthy to mention some significant apparatuses for the interface study in shear loading mode: for example, at the Politechnic University of Marche (Ancona, Italy), they developed the Ancona shear testing research and analysis device (ASTRA) (Canestrari et al. 2013, 2016; Graziani et al. 2017). At EMPA in Switzeland, the Layer Paralell Direct Shear (LPDS) test, which is a modified version of the Leutner test, was developed (Raab, N. Partl 2009). At the University of Limoges the double shear test can apply cyclic shear loading on two parallel interfaces (Diakhaté

et al. 2011, Ktari et al. 2017), and the shear-torque fatigue testing device uses acoustic emission to quantify the complex shear modulus during a test (Ragni et al. 2020, 2021). At the Technical University of Braunschweig, the direct shear test was developed. The apparatus is the cyclic version of the Leutner test (Isailović 2017, 2018).

Diakhaté and his co-authors witnessed the decrease in fatigue life at the interface when there was not sufficient tack coat content (Diakhaté 2011). Inanother research, authors showed the influence of the normal loading on the shear fatigue life at the interface. As expected, a higher compression normal force helps the interface resist longer during shear fatigue tests (Isailović, Falchetto, and Wistuba 2017)

However, the common disadvantage of these apparatuses is the non-homogenous stress and strain (or displacement) fields existing at the interface, which do not allow for the characterization the interface's intrinsic properties.

The 2T3C apparatus developed in ENTPE/University of Lyon allows to apply quasi-homogenous (i) stress and strain field in the two mixture layers and, (ii) the strain fields in layers and displacement gap at the interface. Furthermore, we can have the access to the behaviour at the interface in the overview of a two-layer structure. This means that the apparatus allows to characterise mechanical properties of the interface and also of two bituminous layers. Previous studies showed that the mechanical behaviour at the interface within the small

strain domain is viscoelastic in shear loading mode (Attia 2020, 2021; Tran 2022 (a, b); Tran 2023).

In this study, the thermomechanical fatigue behaviour in the small strain domain of an interface is investigated using the 2T3C apparatus in small strain domain. First, the 2T3C device and tested materials are presented. Then, complex shear modulus tests at five temperatures (from 0 to 40°C) combined with five frequencies (from 0.01 to 1 Hz) are considered to quantify the viscoelastic behaviour of the two layers and the interface. Finally, a shear-torque fatigue test at 10°C and 3 Hz is analysed.

2. 2T3C apparatus to study bituminous interface

As mentioned in the earlier part, one of the advantages of the apparatus is that the stress and strain fields applied in both layers and the stress and displacement fields at the interface are quasi-homogenous. In order for this assumption to be valid, the hollow cylindrical samples wall thickness must be small enough. The outer and inner radii chosen are 86mm and 61mm, respectively. The ratio of the inner radius over the outer one is 0.71, which is within the range of an acceptable homogeneuos assumption. Sayao and Vaid proposed the range of 0.65 to 0.82 (Sayao, Vaid 1991). Tested samples are double-layered hollow cylinders, and the two layers have the approximate heights. The total height of a double-layered hollow cylinder is 125 mm.

The samples are located inside a thermal chamber, which regulates the temperature in a wide range from -20°C to 60°C, which is sufficient for testing a sample made of bituminous mixtures. Two thermal sensors (PT100) are placed on the inner and outer surfaces of the tested sample to monitor temperatures and verify a uniform temperature inside the sample. Two sides of the thermal chamber are built with transparent windows, allowing four cameras to take images from the outside.

The 2T3C apparatus is equipped with a hydraulic press that can impose axial or/and torsion loading either cyclically or monotonically. The greatest axial loading is ±100 kN, and that of torsion is ±2 kN.m. For cyclic loading, the maximal frequency is 10 Hz in tension/compression and torsion. There are two load cells as can be seen from Figure 1, measuring normal force and torsion applied from the press. There are four noncontact sensors. Two of them measure the relative axial displacements of top and bottom caps on two opposite diametral sides of the sample. They allow to obtain the global axial strain (ε_{zzg}) as an avergare value. The two others give the global displacements in the tangential direction ($u_{\theta zg}$) and allow, in the same way, to obtain the global shear strain ($\varepsilon_{\theta zg}$). The global shear strain is used by the press monitoring system to control shear loading during the test (sinusoidal loading). The accuracy of the sensors is 0.1 μm. During the test, the applied axial load is kept constant by the really small compression (-0.026 MPa) and the press's monitoring system.
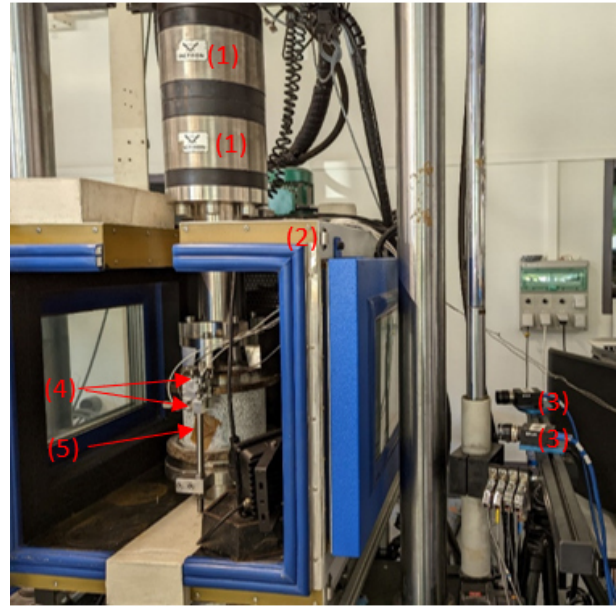

Figure 1. 2T3C apparatus ((1) load cells, (2) thermal chamber, (3) camera system, (4) noncontact sensor groups, (5) thermal sensors)

3. Materials and sample production

3.1. Materials

A sample tested in this study has two layers fabricated from two different bituminous mixtures with an interface made of bitumen emulsion. The two mixtures are BBSG3 0/10 (BBSG in the following figures) for the upper layer with the nominal maximum aggregate size of 10mm and EME2 0/14 for the lower layer with the nominal maximum aggregate size of 14mm (EME in following figures). The gradation curves of two mixtures are shown in Figure 2; 160/220-graded base bitumen with a residual content of 350 g/m².
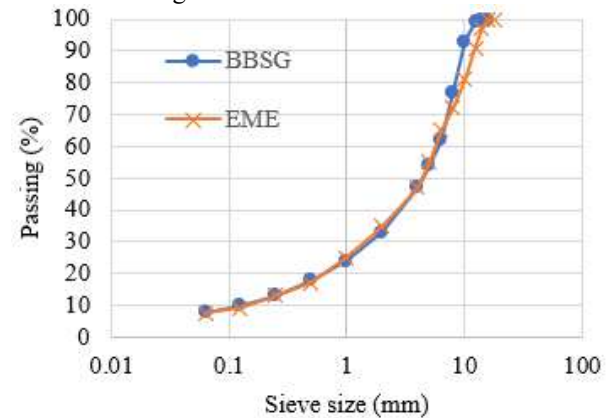

Figure 2. Gradation curves of upper layer BBSG, and lower layer EME

3.2. Sample production

The tested sample was prepared in the laboratory. Double-layered sample production starts with slab fabrication. There are 3 main steps, as illustrated in Figure 3, to produce a double-layered slab. In the first step, the lower layer was compacted with the dimensions of 600x400x75 mm³. The second step was followed after 24 hours of cooling down the lower layer. In this step, a

tack coat was applied on stop of the previous layer, and the slab was left for at least 4 hours for the tack coat to fully brake. In the final step, the top layer is compacted to achieve the total height of a 150 mm double-layered slab.
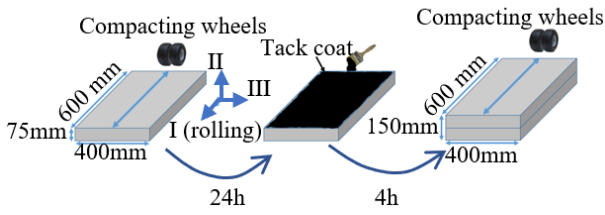
Figure 3. Steps for double-layered slab fabrication

The fabricated slab was left in the laboratory at ambient temperature for few days before coring the samples. The coring stage starts with creating an inner surface of a hollow cylinder (with a dimension of 122 mm) with the smaller drill. Then, the bigger drill was used to extract the sample from the slab, and the dimension of the outer surface of the sample is 172 mm. The sample was then trimmed on its two edges, and the final height is 125mm. There are three samples cored and trimmed from each slab.

In order to use 3D-DIC analysis, a speckle pattern needs to be created on the outer surface of a sample. For that reason, a thin layer of white paint is applied, and black dots are then randomly prayed on top. An illustration is given in Figure 4, which shows the position of three samples in the slab and pictures of a sample before and after speckle pattern application.
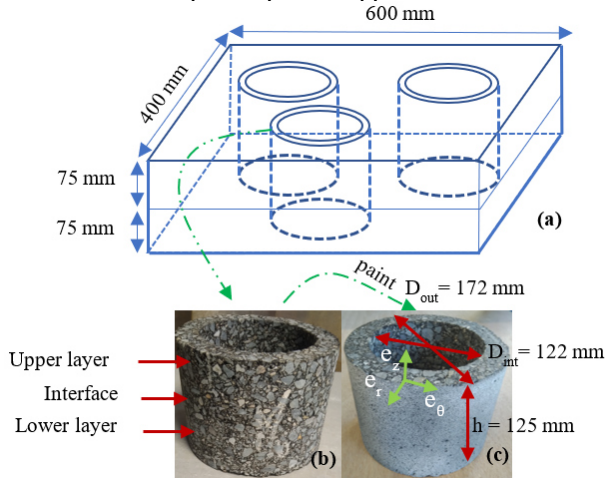
Figure 4. (a) Scheme for double-layered slab and three samples; a sample (b) before speckle pattern application, (c) after speckle pattern application

4. Analysis method and testing procedure

4.1. DIC application, calculation method to obtain strains and displacement gap

The measured displacements from non-contact sensors are global values. In order to distinguish the strain in each layer and the displacement gap at the interface, 3D DIC technology is used. There are two groups of cameras placed outside transparent windows. 50 images are taken by a camera during a loading cycle, except at the loading frequency of 1 Hz where only 35

pictures are taken due to the cameras highest acquisition frequency of 35 images per second. The first image is considered a reference image. The following images are taken at different deformed states of the sample during a loading cycle. At a single time, two cameras in a group take a pair of pictures of the same area of interest; each pair of 2D images is used by the software VIC® 3D to construct a 3D image. The displacements of all points inside an area of interest will be deduced using 3D-DIC technology. One point in the area of interest is represented by a pixel; which is equivalent to 75x75 μm² (technical property of the cameras). A pixel has a grey colour within the greyscale ranging from 0 (total black) to 255 (total white). To insure the accuracy of displacement deduced for a point, a subset with that point in the centre is chosen. The size of a subset is decided at 25x25 pixels². The idea is to have a unique combination of 25x25 pixels², so that subset is easier to search in all deformed states. Algorithms for DIC technology then work on a subset scale, and the deduced relative displacement of the subset between two states is subsequently given back to the points at the centre. The distance between two calculating points is chosen to be 6 pixels.

When all points in the area have their displacements deduced, the shear strain in layers and displacement gap can be calculated as in Figure 5. This calculation method was developed at the Univ. of Lyon/ENTPE. The principle of the method is to create 12 trips (3x100 mm²) in a single layer and calculate the averaged tangential displacement of all trips (u_θ) and plot them in the x axis of a graph against their heights at the centre in the y axis. If the bituminous mixture in each layer is homogenous, there is a linear regression line formed from 12 averaged tangential displacement values for each layer in the graph. The slope of each linear regression line is the shear strain of that layer. Since two different bituminous mixtures are used for the double-layered hollow cylinder sample, there are two linear regression lines with two different slopes. The displacement gap at the interface (Δu_θ) is calculated from the gap between the two lines.
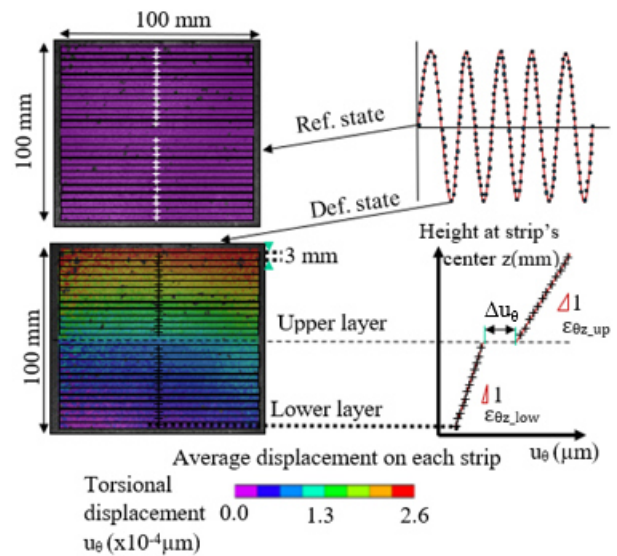
Figure 5. 3D-DIC procedure to find strains in layers and displacement gap at the interface for a deformed state

4.2. Calculation of shear complex modulus in the two layers and complex shear stiffness of the interface

Since stress field is assumed to be homogenous in the sample, the stress is calculated in Eq. (1). T is the torque measured by the load cell, R_{ext} and R_{int} are respectively the outer and inner radius of the sample.

$$\tau_{\theta z} = \frac{3T}{2\pi(R_{ext}^3 - R_{int}^3)} \qquad (1)$$

If the two tested materials and the interface have linear viscoelastic properties, a sinusoidal strain as Eq. (2) leads to a sinusoidal stress as Eq. (3). A phase lag φ_G, which depends on frequency and temperature, exists between the global shear strain ($\varepsilon_{\theta zg}$) and the shear stress ($\tau_{\theta z}$). In Eq. (2), $\varepsilon_{\theta zg\_0}$ is the global shear strain amplitude, $u_{\theta zg\_0}$ is the global tangential displacement amplitude, and $\tau_{\theta z\_0}$ is the stress amplitude in Eq. (3).

$$\varepsilon_{\theta zg} = \frac{u_{\theta zg\_0}}{2h} = \varepsilon_{\theta zg\_0}\sin(\omega t) \qquad (2)$$
$$\tau_{\theta z} = \tau_{\theta z\_0}\sin(\omega t + \varphi_G) \qquad (3)$$

Thanks to 3D-DIC technology and the method developed, the shear strains in upper layer ($\varepsilon_{\theta z1}$) and lower layer ($\varepsilon_{\theta z2}$) are both measured (Eq. (4) and (5), respectively). Where $\varepsilon_{\theta z1\_0}$ and $\varepsilon_{\theta z2\_0}$ are the shear strain amplitudes in the upper and lower layers. In Eq. (4) and (5) α_1 and α_2 are the two measured phase lags.

$$\varepsilon_{\theta z1} = \varepsilon_{\theta z1\_0}\sin(\omega t + \alpha_1) \qquad (4)$$
$$\varepsilon_{\theta z2} = \varepsilon_{\theta z2\_0}\sin(\omega t + \alpha_2) \qquad (5)$$

The displacement gap at the interface (Δu_θ) can be seen in Eq. (6), where Δu_{θ_0} is displacement gap amplitude, and α_Δ is a phase lag.

$$\Delta u_\theta = \Delta u_{\theta\_0}\sin(\omega t + \alpha_\Delta) \qquad (6)$$

Because the stress is homogeneous, the shear stress values in the two layers ($\tau_{\theta z1}$ in upper layer and $\tau_{\theta z2}$ in lower layer) and at the interface ($\tau_{\theta z\Delta}$) are the same ($\tau_{\theta z1} = \tau_{\theta z2} = \tau_{\theta z\Delta} = \tau_{\theta z}$ as shown in Eq. (3))
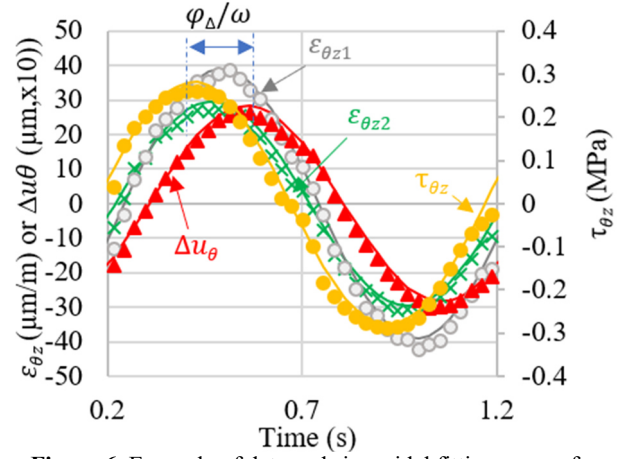
Shear complex moduli in upper and lower layers ($G_{\theta z1}^*$ and $G_{\theta z2}^*$, respectively) are given in Eq. (7) and (8), $|G_{\theta z1}^*|$ and $|G_{\theta z2}^*|$ are their norms. The interface complex stiffness ($K_{\theta z}^*$) is calculated in Eq. (9), $|K_{\theta z}^*|$ is its norm.

$$G_{\theta z1}^* = \frac{\tau_{\theta z\_0}}{2\varepsilon_{\theta z1\_0}} e^{i(\varphi_G - \alpha_1)} = |G_{\theta z1}^*|e^{i(\varphi_1)} \qquad (7)$$
$$G_{\theta z2}^* = \frac{\tau_{\theta z\_0}}{2\varepsilon_{\theta z2\_0}} e^{i(\varphi_G - \alpha_2)} = |G_{\theta z2}^*|e^{i(\varphi_2)} \qquad (8)$$
$$K_{\theta z}^* = \frac{\tau_{\theta z\_0}}{\Delta u_{\theta\_0}} e^{i(\varphi_G - \alpha_\Delta)} = |K_{\theta z}^*|e^{i(\varphi_\Delta)} \qquad (9)$$

Figure 6 shows signals for one cycle obtained from the complex shear modulus test at 10°C, 1 Hz. As can be seen, all the signals are sinusoidal.

Figure 6. Example of data and sinusoidal fitting curves for one cycle signals at 10°C, 1 Hz: $\varepsilon_{\theta z1}$ and $\varepsilon_{\theta z2}$ are the shear strain value in upper and lower layers; Δu_θ is the displacement gap at the interface; $\tau_{\theta z}$ is the shear stress

4.3. Shear complex modulus test

In order to study the thermomechanical behaviour of the interface in shear loading mode, the shear complex modulus tests were launched. The tests consist of applying sinusoidal tangential displacement in the small strain domain. A sample was tested at different combinations of 5 temperatures (0, 10, 20, 30, and 40°C) with 5 frequencies (0.01, 0.03, 0.1, 0.3, and 1 Hz). Figure 7 illustrates the loading history applied to one temperature. The tests were torsional displacement controlled, and the global displacement magnitude was 22.5 μm which corresponds to global shear strain of 50μm/m (when a sample were made with one mixture without an interface in between). This strain was calculated from the relative displacement between non-contact sensors attached to the top cap and their targets attached to the bottom cap. During a complex shear modulus, the normal stress was kept constant at -0.026 MPa. This very small compression has also been applied to glue the sample to the caps.
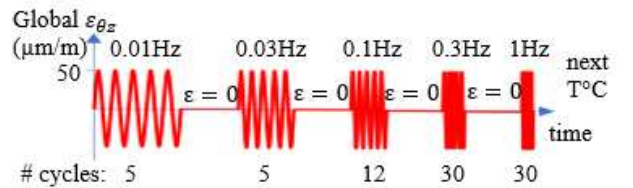
Figure 7. Loading history applied for one temperature in the shear complex modulus (5 temperatures from 0°C to 40°C), there are 5 temperature (from 0°C to 40°C)

4.4. Shear fatigue test

The shear fatigue test is conducted at a frequency of 3 Hz and a temperature of 10°C. The test was controlled in global displacement, which is the same as in shear complex modulus test (22.5 μm). This is the relative tangential displacement ($u_{\theta zg}$) between the top and bottom surfaces of the sample. This relative displacement corresponds to the shear strain ($\varepsilon_{\theta zg}$) of 50 μm/m on the whole sample. The normal force applied to the sample during this shear fatigue test is constant -0.026 MPa.
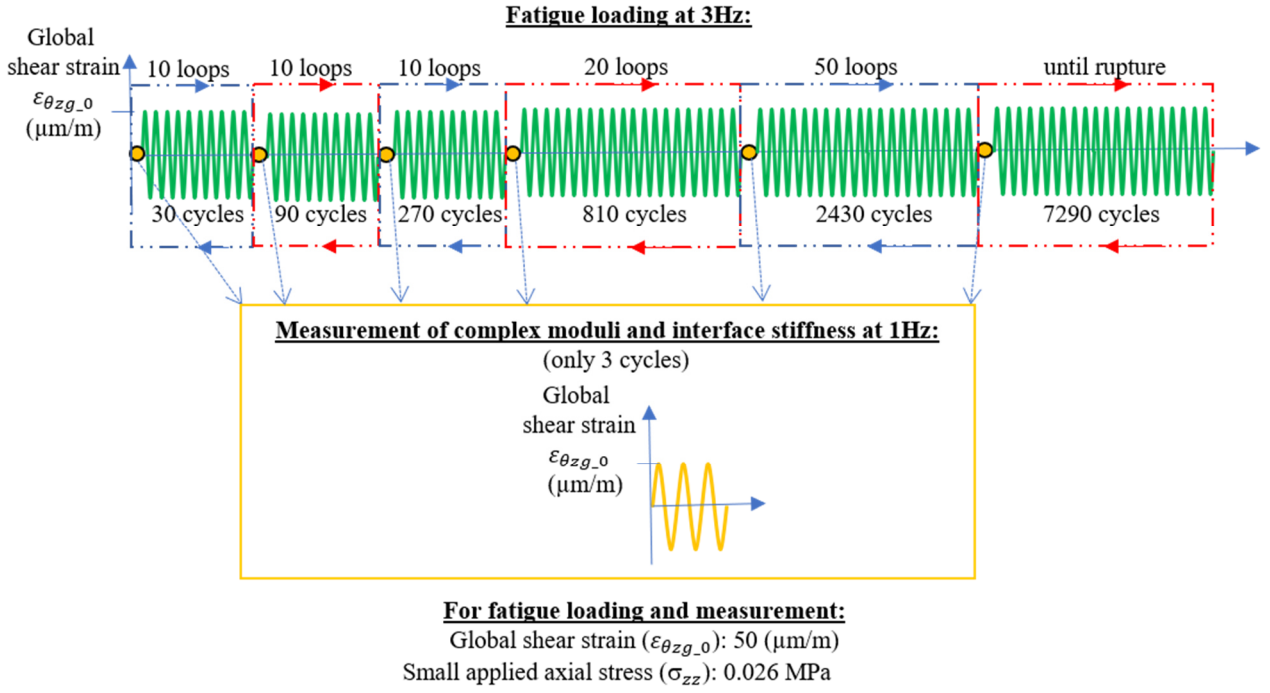
Figure 8. Loading history applied for shear fatigue test procedure (testing temperature: 10°C)

This strain is chosen in order to have a fatigue life of interface from 10^3 to 10^6 (cycles). The characteristics of the camera gives it an accuracy of 0.75 μm. The loading frequency during the fatigue test is 3 Hz, as mentioned, and the highest frequency of cameras is 35 Hz. There will be about 12 photos taken during each loading cycle at 3Hz, and this quantity is not enough for the measurement of complex moduli and interface stiffness. In order to overcome this difficulty, the loading frequency is reduced to 1 Hz when the cameras work. Each time, a camera takes 105 photos, corresponding to three cycles (or three seconds). The shear fatigue test procedure is shown in Figure 8.

5. Results

5.1. Shear complex modulus in layers and stiffness at interface

Figure 9(a) shows master curves for norm of shear complex moduli ($|G^*_{\theta z1}|$ for the upper layer and $G^*_{\theta z2}|$ for the lower layer) and complex interface stiffness $|K^*_{\theta z}|$, while Figure 9(b) presents master curves for their phase angle φ_1, φ_2, and φ_Δ. The master curves are built by multiplying the experimental frequencies of each isothermal curve with their corresponding shift factor indicated in Figure 10. The referent temperature chosen in this paper is 20°C, so experimental frequencies at 20°C multiply by 1. If a viscoelastic material follows Time-Temperature Superposition Principle (TTSP), there are unique master curves for norm and phase angle of complex modulus built. As can be seen from Figure 9 (a) and (b), there are not only unique curves for norm and phase angle of complex shear moduli in two bituminous layers, but also for those of complex shear interface stiffness. This also confirms that the interface shows viscoelastic behaviour in the small strain domain.
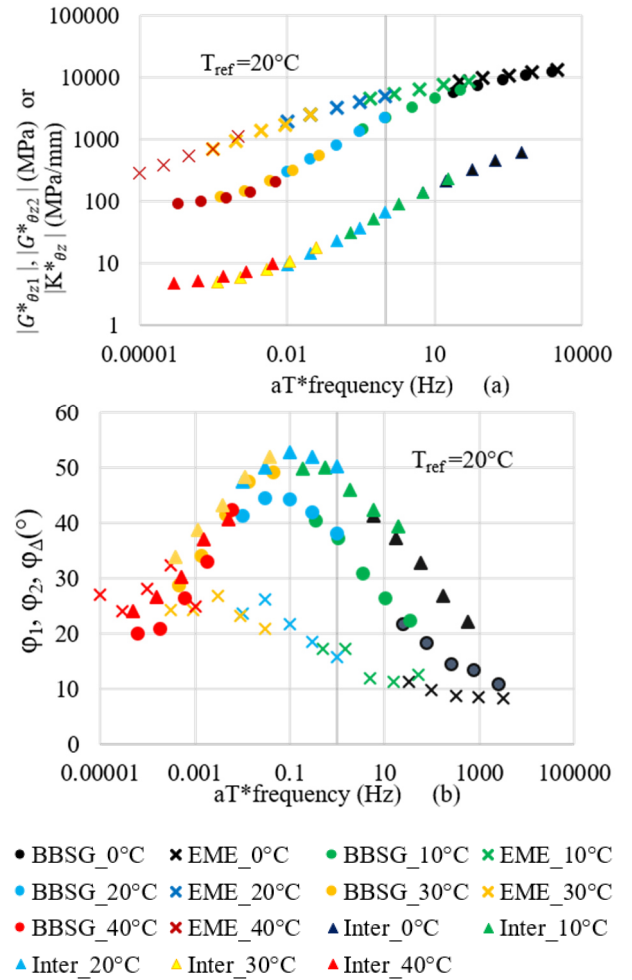

Figure 9. Master curves of (a) norm of shear complex modulus: $|G^*_{\theta z1}|$ and $|G^*_{\theta z2}|$ for upper and lower layers, corresponding; $|K^*_{\theta z}|$ norm of complex interface stiffness of interface; (b) phase angle of shear complex modulus in layers (φ_1, φ_2), and of shear complex shear interface stiffness (φ_Δ).
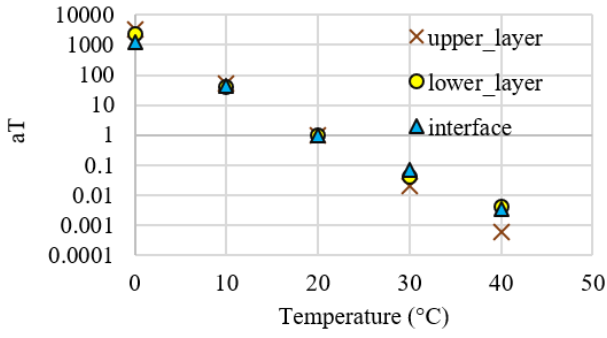
**Figure 10.** Shift factors to build master curves of complex shear modulus/stiffness

5.1. Fatigue behaviour in layers and at interface

The evolution of complex shear moduli for both bituminous layers and the complex shear interface stiffness are shown in the figures below (Figure 11 for their norms and Figure 12 for their phase angle). Norms of shear complex moduli in both layers decrease a bit at the beginning of the test and then maintain constant until the sample is fractured, while the norm of shear interface stiffness reduces constantly for the whole test. The shear stiffness drops significantly in the beginning, then reduces gradually until it approaches constant 37 MPa/mm. The fatigue failure appears at the interface rather than in one of the two layers.
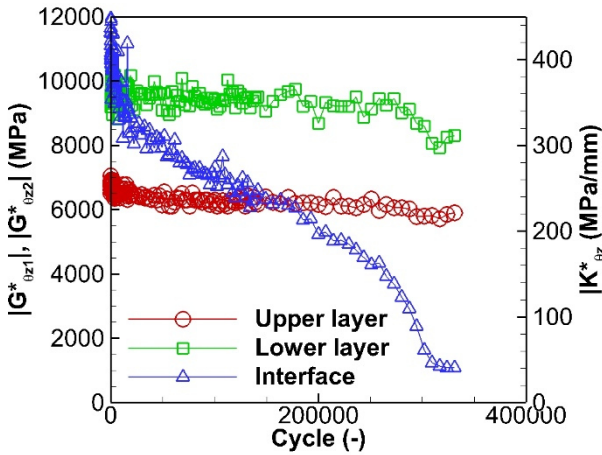

Figure 11. Evolutions of norms of complex shear modulus $|G^*_{\theta z1}|$ and $|G^*_{\theta z2}|$ in upper and lower layer, corresponding; and of complex shear interface stiffness $|K^*_{\theta z}|$ during the fatigue test.

The phase angles witness an opposite trending of shear complex moduli/stiffness which means the phase angle of complex stiffness interface (φ_Δ) increases dramatically, while the phase angles of complex shear moduli (φ_1, φ_2) in two layers rise slightly in the first 10000 cycles. Later, φ_Δ increases quickly, while φ_1, φ_2 in two layers remain constant. The phase angle of interface stiffness (φ_Δ) reaches its maximal value after 300000 cycles, then drops and the sample is separated at the interface. Therefore, the shear fatigue test has more influence at the interface between two bituminous layers than in layers.
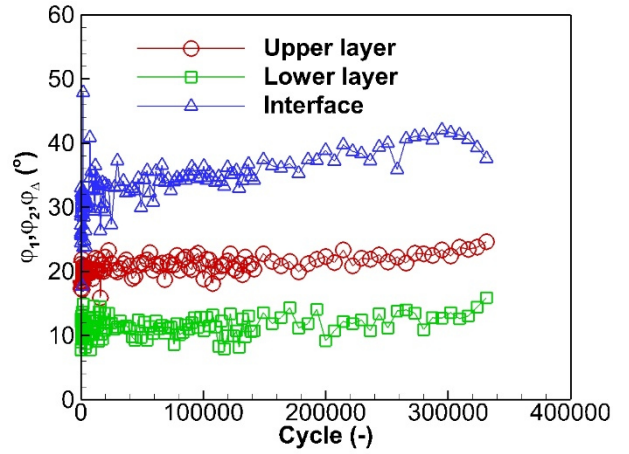
Figure 12. Evolutions of phase angle of complex shear modulus φ_1 and φ_2 in upper and lower layer, corresponding; and of complex shear interface stiffness (φ_Δ) during the fatigue test.

To have a clearer look at the behaviour of the interface, Figure 13 shows the evolution of the displacement gap at the interface between two bituminous layers (Δu_θ) and shear stress during the fatigue test. The displacement gap increases quasi-linearly in the first 200000 cycles, then accelerates at a high speed until failure. On the other hand, the shear stress $(\tau_{\theta z})$ decreases slowly within the first 200000 cycles, then rapidly reduces until the sample is separated at the interface.
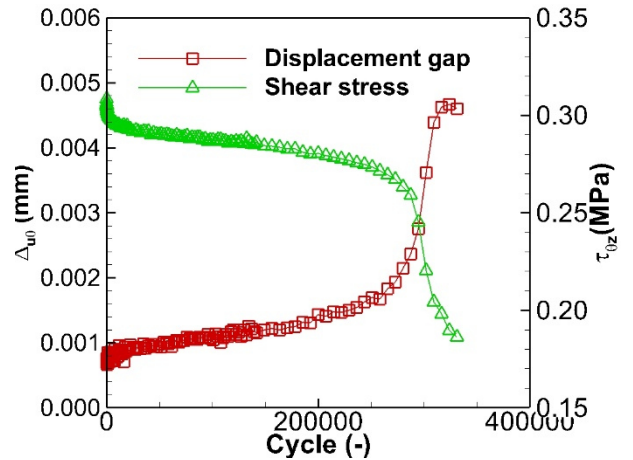
Figure 13. Evolution of displacement gap at the interface (Δu_θ) and shear stress $(\tau_{\theta z})$ inside the sample during the shear fatigue test.

6. Conclusions

In this research, a shear complex modulus test was successfully launched at five different temperatures (from 0°C to 40°C) combined with five different frequencies (from 0.01 Hz to 1 Hz). Furthermore, a shear fatigue test was also performed at a temperature (10°C) and a frequency (3 Hz), some conclusions are withdrawn:

- The apparatus 2T3C can apply sinusoidal torsion to a sample.
- Shear stress in the whole sample, strain in two layers, and the displacement gap at the interface are quasi-homogenous.

- The precision of the camera allows to measure the really small displacement gap at the interface (down to 0.75 μm).
- Time-Temperature Superposition Principle is validated for the mechanical behaviour of two layers and the interface between them.
- The thermomechanical behaviour is viscoelastic not only in the two layers but also at the interface.
- The fatigue failure appears at the interface rather than in the layers. The sample resists the fatigue test until it gets separated at the interface after around 220000 cycles.

Acknowledgements

References

Attia, T.; Di Benedetto, H.; Sauzéat, C., and Pouget S., 2020. "2T3C HCA, a New Hollow Cylinder Device Using Digital Image Correlation to Measure Properties of Interfaces between Asphalt Layers". Constr Build Mat., 247, 118499 https://doi.org/10.1016/j.conbuildmat.2020.118499

Attia, T.; Di Benedetto, H.; Sauzéat, C.; and Pouget S. 2021. "Behaviour of an Interface between Pavement Layers Obtained Using Digital Image Correlation". Mater. Struct. 54 (38): 1–14, https://doi.org/10.1617/s11527-022-01903-1

Canestrari, F. ; G., Ferrotti ; X., Lu ; A., Millien; M. N. Partl ; C., Petit ; A., Phelipot-Mardelé ; H. Piber & C. Raab. 2013. "9th RILEM State-of-the-Art Reports Mechanical Testing of Interlayer Bonding in Asphalt Pavements", RILEM, https://doi.org/10.1007/978-94-007-5104-0_6

Canestrari, F.; Gilda F.; and Graziani, A, 2016. "Shear Failure Characterization of Time–Temperature Sensitive Interfaces". Mech. Time Depend. Mater. 20(3): 405–19. https://doi.org/10.1007/s11043-016-9299-7

Diakhaté, M. et al, 2011. "Experimental Investigation of Tack Coat Fatigue Performance: Towards an Improved Lifetime Assessment of Pavement Structure Interfaces". Constr. Build Mater. 25(2): 1123–33. https://doi.org/10.1016/j.conbuildmat.2010.06.064

Graziani, A.; Canestrari, F.; Cardone, F.; and Ferrotti G.2017. "Time–Temperature Superposition Principle for Interlayer Shear Strength of Bituminous Pavements". Road Mater. Pavement Des. 18(March): 12–25. https://doi.org/10.1080/14680629.2017.1304247

Isailović, I.; Cannone Falchetto, A.; and Wistuba, M., 2017. "Fatigue Investigation on Asphalt Mixture Layers' Interface". Road Mater. and Pavement Des. 18: 514–34. https://doi.org/10.1080/14680629.2017.1389087

Isailović, I.; and Wistuba, M, 2018. "Asphalt Mixture Layers' Interface Bonding Properties under Monotonic and Cyclic Loading". Constr. Build. Mater. 168: 590–97. https://doi.org/10.1016/j.conbuildmat.2018.02.149

Ktari, R; Fouchal, F.; Millien, A.; and Petit, C. 2017. Surface Roughness: A Key Parameter in Pavement Interface Design. European Journal of Environmental and Civil Engineering 21(March): s27–42.

Petit, C. et al 2019. "Pavement Design for Curved Road Sections: Fatigue Performance of Interfaces and Longitudinal Top-down Cracking in Multilayered Pavements". Road Mater. Pavement Des. 10(3): 609–24. https://doi.org/10.3166/rmpd.10.609-624

Raab, C.; Norbert Partl, M.; and Halim, Abd El. "Evaluation of Interlayer Shear Bond Devices for Asphalt Pavements". Balt. J. Road Bridge Eng. 4(4): 186–95, 2009, http://doi.org/10.3846/1822-427X.2009.4.186-195

Raab, C.; Norbert Partl. "Interlayer bonding of binder, base and subbase layers of asphalt pavements: Long-term performance". Constr Build Mater., 23 (2009), 2926-2931, 2009, http://doi.org/10.1016/j.conbuildmat.2009.02.025

Ragni, D.; Ferrotti, G.; Petit, C.; and Francesco Canestrari. 2020. "Analysis of Shear-Torque Fatigue Test for Bituminous Pavement Interlayers". Constr. Build. Mater. 254: 119309, 2020. https://doi.org/10.1016/j.conbuildmat.2020.119309

Ragni D.; Sudarsanan, N.; Canestrari, F.; and Kim, Y. R 2021. "Investigation into Fatigue Life of Interface Bond between Asphalt Concrete Layers". Int. J. Pavement Eng. 0(0): 1–15. https://doi.org/10.1080/10298436.2021.1894420

Sayao, A., and Vaid. Y. P. 1991. "Critical Assessment of Stress Nonuniformities in Hollow Cylinder Test Specimens". Soils Found. 31(1): 60–72, (1991). https://doi.org/10.3208/sandf1972.31.60

Tran, T.N.; Mangiafico, S.; Sauzéat, C.; Di Benedetto,H. 2022a. "Bituminous Interlayers Thermomechanical Behaviour under Small Shear Strain Loading Cycles with 2T3C Apparatus: Hollow Cylinder and Digital Image Correlation". In Eng. Proc. 17, 26. https://doi.org/10.3390/engproc2022017026

Tran, T.N.; Mangiafico, S; Sauzéat, C.; Di Benedetto, H. (2022b). "Characterization of interface between bituminous layers under shear loading cycles using 2T3C apparatus". In the Eleventh International Conference on the Bearing Capacity of Roads, Railways and Airfields, Trondheim, Norway, Volume 2: 477-486. http://doi.org/10.1201/9781003222897-44.

Tran, T.N.; Mangiafico, S; Attia, T.; Sauzéat, C.; Di Benedetto, H (2023), "Linear and nonlinear thermomechanical behaviour of interface between bituminous mixtures layers : results from 2T3C apparatus and modelling". Road Mater. Pavement Des. https://doi.org/10.1080/14680629.2023.2181009